RSC Advances

PAPER

View Article Online
View Journal | View Issue

Cite this: *RSC Adv.*, 2017, **7**, 36516

Dense AuNP/MoS_2 hybrid fabrication on fiber membranes for molecule separation and SERS detection

Yuefeng Zhao,†[a] Xiaoxiao Pan,†[a] Liren Zhang,[b] Yuanyuan Xu,[a] Chonghui Li,[a] Jundong Wang,[a] Jiayu Ou,[a] Xianwu Xiu,[ac] Baoyuan Man*[a] and Cheng Yang*[ac]

Received 17th May 2017
Accepted 6th July 2017

DOI: 10.1039/c7ra05568d

rsc.li/rsc-advances

Synthesis of uniform and dense metal nanostructures on the whole exposed fiber, instead of simply on the membrane surface, is necessary for controllable separation and sensitive SERS detection. Herein, uniform and dense AuNP/MoS_2 hybrids were synthesized on single 3D glass fiber (GF) surfaces, obtained by the reaction of a MoS_2 nanosheet and $HAuCl_4$. The chemical mechanism (CM) of the MoS_2 layers and the electromagnetic enhancement (EM) of the dense AuNPs were used to enhance the SERS sensitivity. The molecule-separation ability of the obtained GF membranes, constructed by numerous compacted fibers with dense AuNP/MoS_2 hybrids, was not destroyed, and herein, these membranes were used to separate mixed molecules. These MoS_2-based hybrid substrates show great potential for excellent paper-based separation and are sensitive SERS substrates for biological and chemical detection.

Introduction

Surface-enhanced Raman scattering (SERS) is an ultrasensitive vibrational spectroscopic technique that is able to detect molecules on or near the surface of plasmonic nanostructures, with the mechanism of the long-range electromagnetic enhancement (EM) and short-range chemical enhancement (CE).[1] SERS, which integrates high levels of sensitivity with spectroscopic precision, has tremendous potential for chemical and bio-molecular sensing.[2–4]

In principle, SERS is thought to provide unique identification of a target analyte even in the presence of multiple analytes. However, identification of a targeted analyte in complex real-world samples may be challenging due to overlapping of spectral signatures from different analytes as well as interference by highly fluorescent molecules that may be present.[5] Therefore, a combination of separation and SERS detection is necessary to detect multiple targets in practice. At present, the combination of separation and SERS detection of mixed molecules is widely used in drug discovery,[6] determination of synthetic colors,[7] and selective detection of toxic heavy metals.[8] There are many separation methodologies available today including gas and liquid chromatography,[9,10] capillary electrophoresis,[11] and paper chromatography.[12] In this study, we chose paper chromatography due to its features such as simple sample collection, less time-consumption, and pre-analytical treatment. Paper chromatography is a technique that is used for separating target analytes from complex samples, allowing the definite and unambiguous identification of individual analytes from the sample. The combination of paper separation and SERS detection becomes an effective technique. For example, Hyukjin Jung reported the use of cellulose fiber decorated with silver nanoislands for the separation and detection of small molecules.[13] Further enhancements in the SERS sensitivity and separation ability are useful for the application of this technique.

Recent studies indicate that MoS_2 can be an ideal platform to support SERS activity because of its many advantages. First, MoS_2 can provide chemical enhancement and efficient adsorption for various target molecules; hence, the sensitivity of the substrate is enhanced. Second, MoS_2 has chemical stability and can be obtained at low temperatures; these features endow the substrate with a long lifetime and effectively reduce energy consumption.[14,15] Third, the MoS_2 nanosheet exhibits high surface area that makes it a promising supporting material to stabilize metal nanoparticles and form hierarchical composites.[16]

Note that AuNPs can be grown *in situ* on the surface of MoS_2 nanosheets by a spontaneous redox reaction with tetrachloroauric acid ($HAuCl_4$) without any reducing agent.[17,18] The density and diameter of the AuNPs can be controlled by changing the conditions of the reaction between the MoS_2 nanosheet and $HAuCl_4$ to acquire the best SERS-active substrate. AuNPs can concentrate light into small volumes; this greatly enhances the local electromagnetic field near the metal nanostructures.[19] The areas with greatly enhanced EM field become hot spots for surface-enhanced Raman

[a]*School of Physics and Electronics, Shandong Normal University, Jinan 250014, People's Republic of China. E-mail: chengyang@sdnu.edu.cn; byman@sdnu.edu.cn*
[b]*College of Information Technology, UAE University, Al-Ain, United Arab Emirates*
[c]*Institute of Materials and Clean Energy, Shandong Normal University, Jinan 250014, People's Republic of China*
† These authors contributed equally.

spectroscopy.[20] The localized surface plasmon resonance (LSPR) generated on AuNPs induces strong plasmon-exciton coupling, resulting in strong light–matter interaction, thereby enabling enhanced Raman scattering.[21] In addition, AuNPs are well known for their excellence in biocompatibility and less susceptible to oxidation than most of the other SERS-active nanoparticles.[22,23]

Glass fiber (GF) membrane is a good candidate for paper-based SERS substrate as its inner 3D structure is constructed by numerous compacted fibers, with a fine capillary structure, and it is tolerant to biochemical or chemical circumstances.[24] Compared to monolithic substrates, the glass fiber offers a large surface area for adsorption due to its 3D structure and immobilizes SERS-active nanoparticles onto the interior surface of the capillary to avoid floating of the nanoparticle aggregates on the surface; this can highly improve reproducibility, enhance Raman signals of molecules, and extend its application.[25,26] In addition, GF membranes composed of intricate fibers allow paper chromatographic separation under the action of capillary effect, which are feasible for the separation and pre-concentration of analytes from a complex substrate. Paper, as a substrate, has been used for the separation and detection of complex samples. However, the structure of paper is not sufficiently uniform; this reduces the speed of sample separation. Moreover, paper as a substrate cannot withstand high temperatures; this limits its scope of application. In this study, GF with a relatively uniform structure and high temperature resistance provided unique capabilities for the two-dimensional chromatographic separation and SERS detection.

In this study, we selected crystal violet (CV) and toluidine blue (TB) as probe molecules to analyze the performance of the substrate. As is known, CV and TB dyes are much studied fluorescent probe molecules with numerous applications in biology and biochemistry. CV and TB have different polarities; hence, they can be spatially isolated on the GF substrate based on their different affinities for the stationary and mobile phases.[27] We introduced a highly practical and sensitive sensor, GF-MoS_2@AuNP substrate, that provided a new platform for the label-free screening and ultrasensitive detection of the mixture of CV and TB molecules.

Methods

Reagents and materials

All chemicals, including ammonium tetrathiomolybdate $(NH_4)_2MoS_4$, dimethylformamide (DMF), chloroauric acid ($HAuCl_4$), crystal violet (CV), toluidine blue (TB), ethanol (99.7%), and glass fiber, were directly used without further purification.

Preparation of the GF-MoS_2@AuNP substrate

Large-scale growth of few-layered MoS_2 was achieved by thermally decomposing the precursor ammonium tetrathiomolybdate ($(NH_4)_2MoS_4$). High-purity $(NH_4)_2MoS_4$ (0.01 g) was added to 1 mL dimethylformamide (DMF) to form a solution. The solution was sonicated for 40 min before use. A glass fiber was immersed in the $(NH_4)_2MoS_4$ solution and then naturally dried.

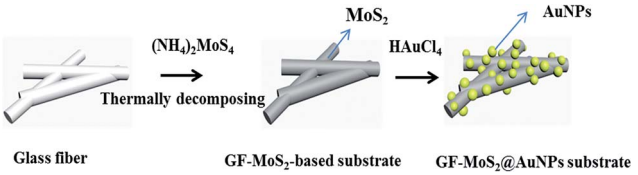

Fig. 1 Schematic of the synthesis of the GF-MoS_2@AuNP substrate. The precursor $(NH_4)_2MoS_4$ was dip-coated on the substrate. The thermal decomposing process was performed in a quartz tube furnace. AuNPs grew *in situ* on the surface of the MoS_2 nanosheet by a spontaneous redox reaction between the MoS_2 nanosheet and tetrachloroauric acid ($HAuCl_4$).

The prepared glass fiber was placed in a tube furnace under a flow of a gas mixture of Ar/H_2 at the flow rate = 4/1 sccm. MoS_2 was formed on the glass fiber *via* thermal annealing at 500 °C for 90 min. Raman spectra were obtained *via* the HORIBA HR800 Raman microscopy system (HORIBA, Kyoto, Japan) (laser wavelength 532 nm, objective lens magnification 50, and laser power 1%) to determine the presence of MoS_2. AuNP-decorated MoS_2 nanocomposite was synthesized *via* a direct reaction between MoS_2 and $HAuCl_4$. The morphology of the sample was characterized using a scanning electron microscope (SEM, Zeiss Gemini Ultra-55, Carl Zeiss, Inc., Oberkochen, Germany). The complete process for the construction of the GF-MoS_2@AuNP substrate is shown in Fig. 1.

Separation of the mixture

Crystal violet (CV) and toluidine blue (TB) solutions were prepared using deionized water and spotted separately on the glass fiber using a capillary tube with a volume of 5 μL. The mixed solution of CV and TB was then spotted on the glass fiber using the same procedure. Paper separation was developed using 99.7% ethanol as a mobile phase. After being dried under ambient conditions, the glass fiber was suspended in a beaker with ethanol for pre-saturation. Pre-saturation took about 15 min. Then, the bottom of the glass fiber was immersed in ethanol. The separation effect of the mixed molecules was analyzed *via* colorimetric detection of dye molecules.

Results and discussion

GF membranes were used as substrates for the growth of MoS_2 by the thermal decomposition method due to their high temperature resistance. Chemical reduction between MoS_2 and $HAuCl_4$ realizes the deposition of dense AuNPs on the glass fiber. The GF-MoS_2@AuNP substrate allows highly sensitive detection of CV and TB molecules, and its morphology is characterized by SEM. The SEM images of the glass fiber, glass fiber with MoS_2, and gold nanoparticle-loaded glass fiber are shown in Fig. 2. Fig. 2a displays the morphology of the glass fiber at different magnifications, and the inset shows the magnified SEM image. The GF membrane is formed by many wire-type glass fibers with different diameters that can trap the precursor and act as the initial nucleation centers for the growth of the AuNPs. In addition, a relatively uniform color is obtained,

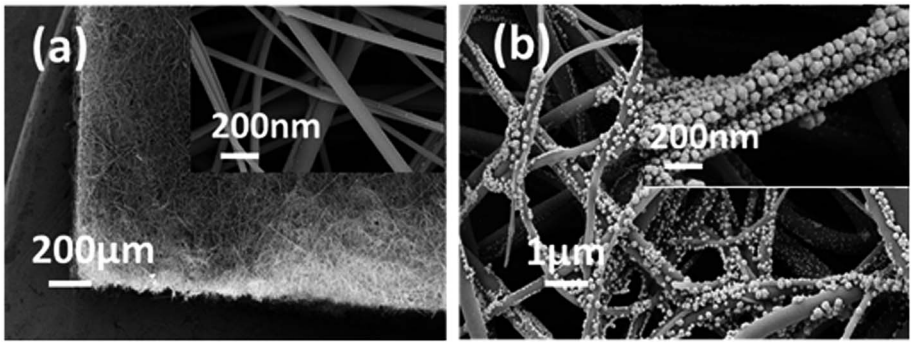

Fig. 2 (a) SEM images of the GF membranes at different magnifications. (b) SEM images of the GF-MoS_2@AuNP substrate. The inset is the SEM image of the GF-MoS_2@AuNP substrate at high magnification.

and no rippled or wrinkled structures are detected on each glass fiber. Fig. 2b is the SEM image of the GF-MoS_2@AuNP substrate, and a large number of AuNPs (about 50 nm in diameter) attached to the GF membranes can be clearly seen in the inset.

Fig. 3 illustrates the numerical results of Raman spectra with peaks at 377 cm^{-1} and 408 cm^{-1} attributed to E^1_{2g} and A_{1g}, respectively. The E^1_{2g} (in-plane) mode results from opposite vibrations of two S atoms with respect to the Mo atom, and the A_{1g} mode is associated with the out-of-plane vibration of S atoms in opposite directions.[28] After successful synthesis of the GF-MoS_2@AuNP substrate, we obtained the Raman spectrum of MoS_2 on the GF membranes (red line) and GF-MoS_2@AuNPs (black line). In Fig. 3a, it can be observed that the Raman signals of MoS_2 molecules slightly increase when it is decorated with AuNPs; this indicated a better enhancement effect of the AuNPs. In the following Raman analysis, CV and TB solutions with different concentrations were used to evaluate the SERS performance of the substrate. In addition to the concentration, the absolute amount of the analyte greatly influences the Raman spectra of the substrate. Therefore, we used analytes with the same volume in each Raman analysis. To operationalize rapid diagnosis tests in clinics, all Raman spectra were obtained by adding traces of analytic samples instead of conventional immersion in solution for long periods of time. No characteristic scattering peaks of CV can be observed except the strong fluorescent background on GF membranes, as shown in Fig. 3b. Both the GF-MoS_2@AuNP and MoS_2 substrates show the Raman enhanced effect toward the CV molecule. All these three substrates show Raman intensity at 914 cm^{-1} and 1620 cm^{-1} toward CV; this results indicates that GF-MoS_2@AuNP substrate displays the best SERS performance. The synergies of charge-transfer, plasmon and exciton, and dipole–dipole coupling of the MoS_2 film cause enhancement in the SERS signal. Therefore, the substrate with MoS_2 shows better SERS effect as compared to the blank GF membranes. However, it is worth noting that the SERS intensity of the GF-MoS_2@AuNP substrate is much stronger than that of the MoS_2 substrate. The presence of AuNPs greatly enhances the local electromagnetic (EM) field near the nanoparticles. In addition, AuNPs can excite surface plasmons and produce strong scattering spectra, thus amplifying the Raman signal. Therefore, the CV molecule on the GF-MoS_2@AuNP substrate displays the most intense characteristic scattering peaks.

The density and size of the AuNPs can be easily controlled by changing the reaction time and keeping other conditions unaltered, which influence the SERS properties of the substrate. We chose 3 min as a time interval and increased the time of the reaction between MoS_2 and $HAuCl_4$ from 3 to 15 min. Fig. 4 shows the SEM images of the GF-MoS_2@AuNP substrate

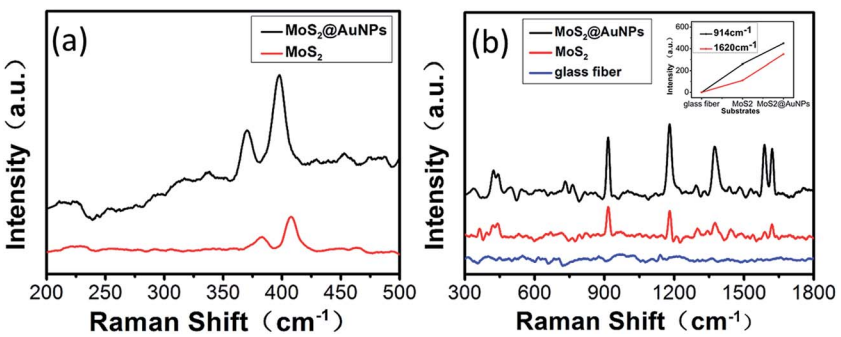

Fig. 3 (a) Raman spectrum of MoS_2 on GF membranes (red line) and GF-MoS_2@AuNPs (black line). The peaks at 377 cm^{-1} and 408 cm^{-1} are attributed to E^1_{2g} and A_{1g}, respectively. Raman signals of the MoS_2 molecules slightly increase when it is decorated with AuNPs. (b) The Raman spectrum of CV with a concentration of 10^{-4} M on different SERS-active substrates. Both GF-MoS_2@AuNPs substrate and substrate only with MoS_2 have SERS effects for CV, and the former shows better performance. The inset is the Raman intensity of the CV molecules at 914 cm^{-1} and 1620 cm^{-1} for various SERS-active substrates.

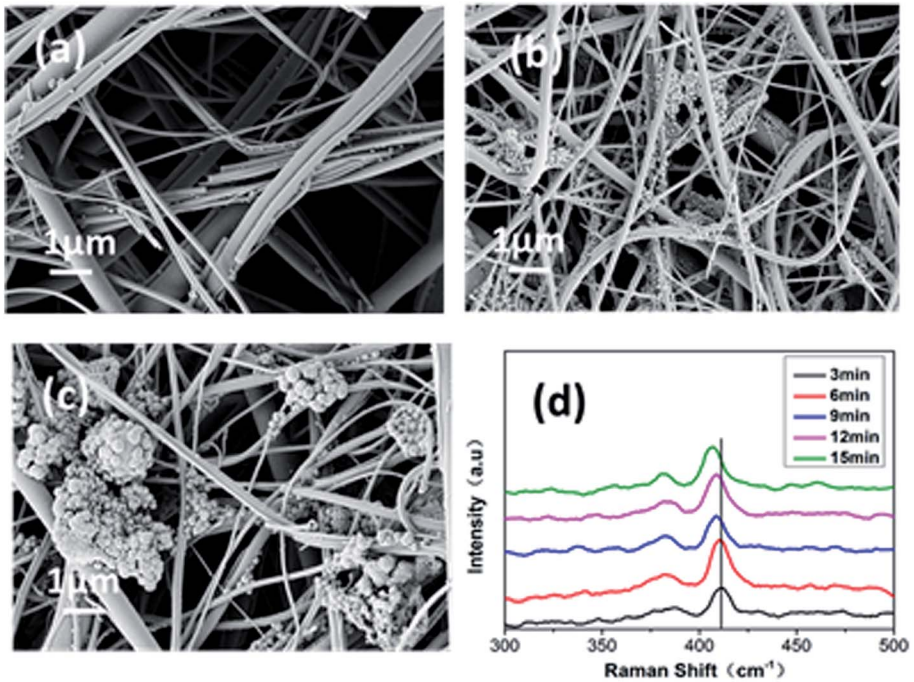

Fig. 4 SEM images of the GF-MoS_2@AuNP substrate obtained at different reaction times: (a) 3 min; (b) 9 min, and (c) 15 min. (d) The Raman spectrum for MoS_2 treatment at 3 min, 6 min, 9 min, 12 min, and 15 min.

obtained at various reaction times. As shown in Fig. 4a, when the reaction time is 3 min, only few and small nanoparticles are formed as seeds on the surface of the GF membranes or at the gap between fibers. As the time increases, AuNPs become larger in size and more in number, and a high-density AuNP-decorated MoS_2 nanocomposite is obtained at 9 min; however, most of the AuNPs are distributed in the intersection of fibers (Fig. 4b). When the reaction time is increased to 15 min, AuNPs grow larger and become aggregated (Fig. 4c) because with continuous reactions between $HAuCl_4$ and MoS_2, Au ions in the solution become reduced by the active nucleation sites and result in anchoring of AuNPs on these sites. Several AuNPs come together to form a large particle; this leads to the exposure of fibers. With the continuous reaction between MoS_2 and $HAuCl_4$, the number of layers of the MoS_2 films changed. Fig. 4d shows the Raman spectrum of MoS_2 with different reaction times. Note that the A_{1g} peak undergoes a blue shift, whereas the E^1_{2g} peak undergoes a slightly red shift; this suggests that the number of MoS_2 layers decreases with the increase in the reaction time. This may be because S–Mo–S bonding in MoS_2 is not strong enough and the interlayer interaction between MoS_2 layers is weak. Continuous chemical reactions between MoS_2 and $HAuCl_4$ lead to defects in MoS_2 and then decrease its thickness.

To explore the SERS performance of the GF-MoS_2@AuNP substrates at different reaction times, the Raman spectrum of all substrates towards CV with a concentration of 10^{-4} M is shown in Fig. 5a. The time of the reaction between MoS_2 and $HAuCl_4$ has a significant impact on the SERS properties of the GF-MoS_2@-AuNP substrate. The SERS intensity is weaker when the reaction time is short. The reason is that the number of AuNPs is small, and hence, the hot spots on the substrate are very less. The SERS intensity becomes much stronger with the increase in the reaction time because AuNPs are dense and less aggregated, which can generate more hot spots. The SERS effect of the substrate depends on the AuNP size and density. With further increase in the reaction time, AuNPs seriously aggregate and move far away from other gold nanoclusters; this reduces the number of hot spots and weaken the SERS intensity.[29] According to previous studies, the SERS performance is also affected by the number of MoS_2 layers; thinner MoS_2 shows better SERS performance. As the CV peak near 914 cm^{-1} is more representative and its intensity is very sensitive, according to the spectra, it is selected as the representative peak to evaluate the sensitivity of different substrates. Fig. 5b demonstrates that the GF-MoS_2@AuNP substrate produces the best effect of Raman enhancements when the reaction time is 9 min not only because it has dense particles but also because it has a thinner MoS_2 layer.

Although the extension of the reaction time can enhance the SERS effect of the substrate to a certain extent, continuous reactions between $HAuCl_4$ and MoS_2 reduce the number of hot spots and affect the Raman enhancement of the substrate. Through further research, we found that multiple repetitions of chemical reactions between MoS_2 and $HAuCl_4$ could control the sizes of the deposited nanoparticles and greatly enhance the SERS effect. We proposed a power-free method to densely and uniformly deposit AuNPs on glass fiber; this method is similar to the successive ionic layer absorption and reaction (SILAR) method.[30] This method provided control over the size of particles *via* a number of chemical treatment cycles. Compared with other methods, in this method, multiple repetitions of chemical reactions produce evenly distributed AuNPs and reduce the polymerization of AuNPs. We again chose 3 min as a time interval

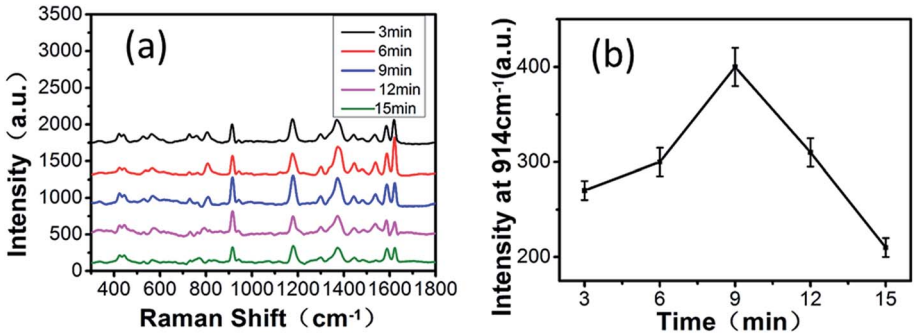

Fig. 5 (a) Raman spectrum of the CV molecules on different GF-MoS_2@AuNP substrates obtained when the time of the reaction between MoS_2 and $HAuCl_4$ is increased from 3 to 15 min. As time increases, the SERS effect of the substrate changes constantly. (b) Raman intensity of CV molecules at 914 cm^{-1} for various substrates. The GF-MoS_2@AuNP substrate shows the best SERS performance when the reaction time is 9 min.

again to achieve multiple AuNP deposition. For the first cycle, the MoS_2 substrate was immersed in $HAuCl_4$ solution and treated for 3 min; then, it was removed and rinsed with deionized water to wash out the non-reacted residues to obtain the GF-MoS_2@AuNP-1 substrate. Then the GF-MoS_2@AuNP-1 nanocomposite was immersed in $HAuCl_4$ solution again for the same reaction time to produce GF-MoS_2@AuNP-2. Next, we increased the number of chemical treatment cycles to obtain GF-MoS_2@AuNP-3, GF-MoS_2@AuNP-4, and GF-MoS_2@AuNP-5. Fig. 6a is the SEM image of the GF-MoS_2@AuNP-2. AuNPs on GF-MoS_2@AuNP-3 are significantly increased, but nanoparticles are gathered in the intersection of fibers and inhomogeneously distributed (Fig. 6b). Compared to Fig. 4b, which is an SEM image obtained at 9 min, Fig. 6c shows GF-MoS_2@AuNP-4 with high density and uniform distribution of AuNPs. AuNPs begin to cluster (red box in Fig. 6d) and the surface of the GF membranes is exposed as described earlier. The AuNPs produced in the first cycles act as seeds and their quantity and diameters are gradually increased *via* a synthesis reaction that occurred at the seeds through multiple repetitions. The electrostatic repulsion of the charged surface can make the AuNPs stable in solution. However, the lack of sufficient surface charge and stabilizing agent for our products do not prevent the AuNPs from aggregating. Compared with the SILAR method, *via* the proposed method, we synthesized a layered structure of MoS_2 sheets with AuNPs on GF membranes. GF membranes with a more uniform structure and higher temperature resistance compared to paper can be widely applied in rapid detection and analysis under on-site conditions. We

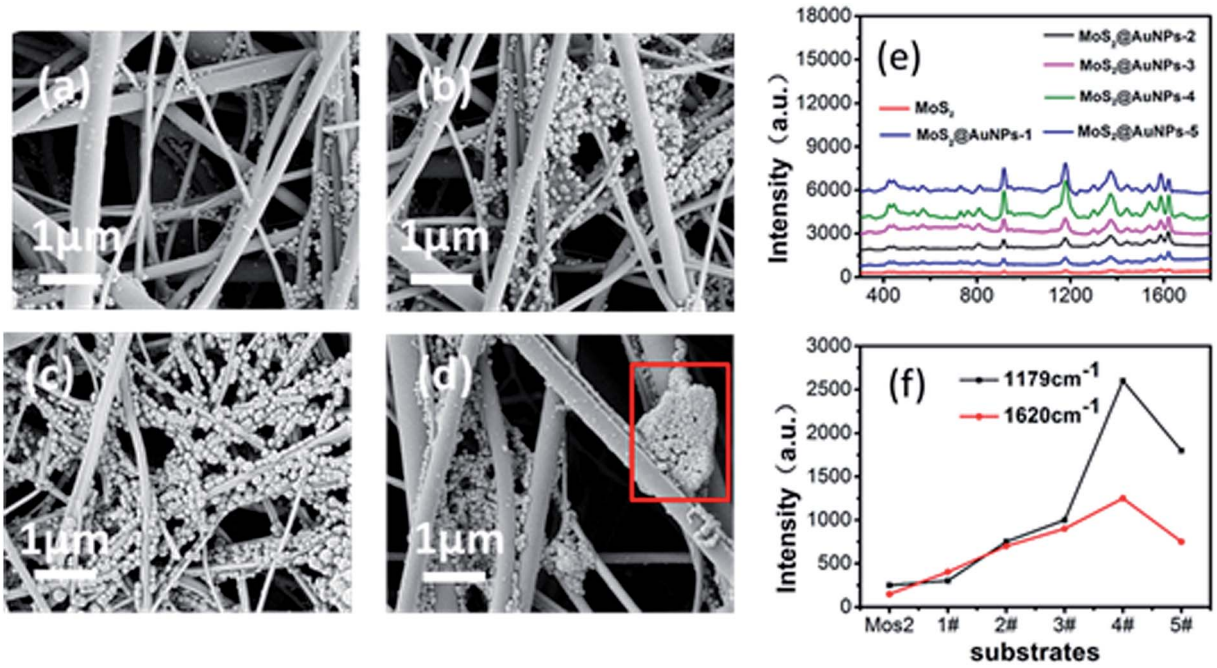

Fig. 6 (a)–(d) SEM image of MoS_2@AuNP-2, MoS_2@AuNP-3, MoS_2@AuNP-4, and MoS_2@AuNP-5. (e) Raman spectrum of CV with a concentration of 10^{-4} M on different substrates. (f) Raman intensity of the CV molecules at 1179 cm^{-1} and 1620 cm^{-1} for various substrates. Both Raman peaks show highest intensity for the GF-MoS_2@AuNP-4 substrate.

produced MoS_2 layers on GF membranes primarily *via* the CVD method rather than directly synthesizing metal nanoparticles on the substrate. In addition to the Raman enhancement effect, MoS_2 can firmly adsorb metal nanoparticles and reduce background fluorescence during detection. MoS_2 shows great ability in redox chemistry, and it can directly react with $HAuCl_4$ to allow a straightforward and green synthesis of AuNPs. Unbound sulfurs act as sites in Au nuclei seeding and growth, and the total rate of assembly of AuNPs is governed by the rate of diffusion of Au ions into the MoS_2 surface and the rate of Au incorporation into the crystalline particles. When MoS_2 film is repeatedly immersed in solution, the introduction of high defect density facilitates a large diffusion coefficient. This reduces the polymerization of nanoparticles and provides more hot spots.[22] For comparison, the CV molecules (10^{-4} M) were also deposited onto the 9 min-treated substrate and five substrates above-mentioned for Raman detection under the same condition (Fig. 6e). Compared with the Raman spectroscopy of the 9 min-treated substrate, the enhancement effect of substrates is greatly improved by the number of chemical treatment cycles; this indicates that multiple AuNP deposition can greatly increase the SERS effect of the substrates. To compare the Raman enhancement magnitude, we chose the SERS intensity of CV on different substrates at the selected low obvious Raman peaks (1179 cm^{-1} and 1620 cm^{-1}). The data are obtained from at least five different locations of the substrate. From Fig. 6f, we discovered that on increasing the number of chemical treatments cycles, the SERS activity was enhanced until four cycles. Moreover, both Raman peaks show highest intensity on the GF-MoS_2@AuNP-4 substrate, indicating that this substrate shows the best SERS performance for CV.

GF-MoS_2@AuNP-4 substrates are exposed to CV and TB solutions of different concentrations, and Raman spectra of CV and TB are shown in Fig. 7a and b, respectively. The blank spectra are the Raman spectra where there is no CV or TB, and there are only two Raman peaks belonging to MoS_2. It can be observed that the detection limit of GF-MoS_2@AuNP substrate for CV is 10^{-8} M. By contrast, the limit for TB detection is lower than 10^{-7} M as TB has good signal-to-noise ratio and its main peaks are still observable at the Raman spectra of 10^{-7} M. Hence, it is obvious that the GF-MoS_2@AuNP-4 substrate is able to improve the detection sensitivity for both CV and TB molecules. Considering the fact that the surface enhancement factor (EF) is one of the most important parameters for characterizing the SERS effect, in this study, the EF of the GNP film is calculated based on the following equation:

$$\mathrm{EF} = (I_{\mathrm{SERS}}/I_{\mathrm{Raman}})(C_{\mathrm{Raman}}/C_{\mathrm{SERS}})$$

where I_{SERS} is the Raman intensity obtained for the SERS substrate at a certain concentration; I_{Raman} is the Raman intensity obtained under non-SERS conditions; C_{Raman} and C_{SERS} represent the CV solution concentrations deposited onto the GF and the GF-MoS_2@AuNP-4 substrate, respectively. Herein, we chose the 1620 cm^{-1} peak of the CV molecule as the reference peak. Using the data shown in Fig. 7a, an EF of 1.3×10^6 is determined ($C_{\mathrm{SERS}} = 10^{-8}$ M and $C_{\mathrm{Raman}} = 10^{-2}$ M). To further investigate the SERS performance of the GF-

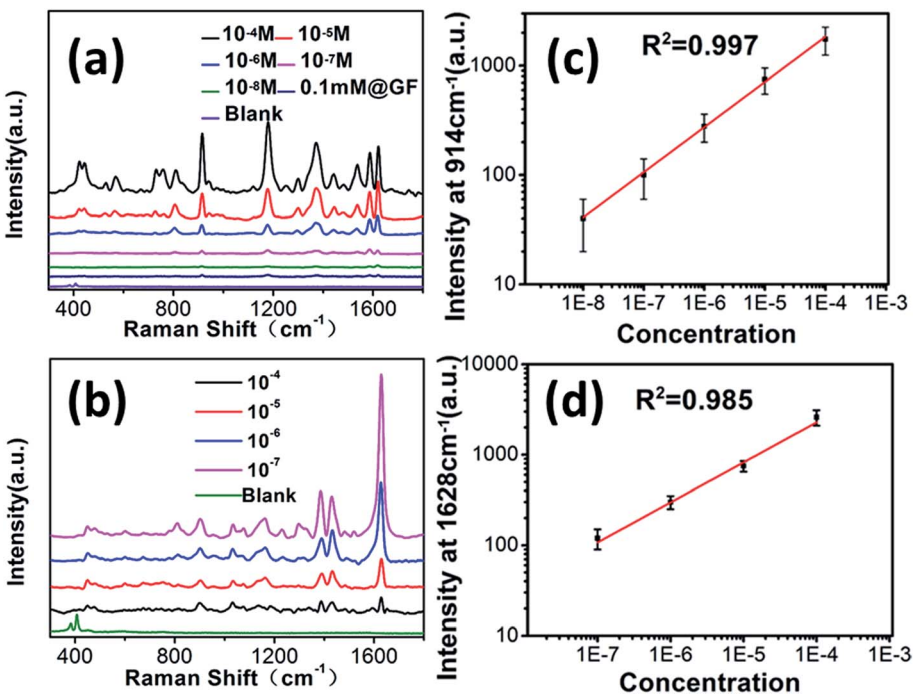

Fig. 7 (a) SERS spectra of the CV molecules with different concentrations. (b) SERS spectra of the TB molecules with different concentrations. (c) Raman intensity of the CV molecules at 914 cm^{-1} for various concentrations. (d) Raman intensity of the TB molecules at 1631 cm^{-1} for various concentrations.

MoS_2@AuNP-4 substrate, Raman peaks located at 914 cm^{-1} and 1631 cm^{-1} are chosen as signatures to determine the concentration of CV and TB in the samples. From Fig. 7c, it can be seen that the Raman intensity of CV molecules at 914 cm^{-1} is linear when the SERS signal ranges from 10^{-4} to 10^{-8} M. In this case, the value of R^2 is 0.997. Similarly, Fig. 7d shows that the Raman intensity of TB molecules at 1631 cm^{-1} is linear when the SERS signal ranges from 10^{-4} to 10^{-7} M and R^2 reaches 0.985. Furthermore, it can be seen that for both CV and TB molecules, the intensity of peaks decreases linearly as the concentration decreases. Therefore, the GF-MoS_2@AuNP-4 substrate is an effective approach that can be applied to quantitatively detect both the CV and TB molecules.

For application purposes, SERS substrates are required to have good stability and reproducibility during the Raman measurements. Fig. 8a–c show the SERS spectra of 10^{-5} M CV adsorbed on the GF-MoS_2@AuNP-4 substrate, which are obtained for five different spots on three different parts of the structure. As seen, although there is a slight variability of the intensity, the characteristic scattering peaks of CV can be detected on all spots. To investigate the stability of the GF-MoS_2@AuNP-4 substrate, the CV concentration of 10^{-5} M is selected to compare the stability of the substrates. The Raman intensity is measured every five days at room temperature. As shown in Fig. 8d, the Raman intensity of the peaks at 914 cm^{-1} and 1620 cm^{-1} is attenuated with the increase in the number of days, and the attenuation of the Raman intensity becomes weak after 10 days. The average intensity of the peak at 914 cm^{-1} is dropped by 36% and the average intensity at 1620 cm^{-1} is decreased only by 28%. Through this analysis, we can conclude that this substrate shows high repeatability and long-term stability. Thus, the GF-MoS_2@AuNP-4 substrate is a good candidate for practical analytical applications of SERS.

The previous substrate synthesized *via* the SILAR method was used only as a SERS platform; however, the GF-MoS_2@AuNP-4 substrate shows great potential in excellent paper chromatographic separation and is a sensitive SERS substrate for biological and chemical detection. Rapid screening of mixed small molecules has been achieved by the method of paper chromatographic separation. GF membranes are porous, and ethanol as a mobile phase can quickly spread under the action of capillary tension. As CV and TB molecules have different distribution coefficients in alcohol and water, with the spread of alcohol, they move at different speeds on the fiber to achieve separation. Colorimetric detection of dye molecules (CV, TB, and their mixed solution 10^{-4} M) after paper separation on GF membranes is shown in Fig. 9a. Points 1 and 2 are the CV and TB molecules after they moved up with the spread of alcohol. Mixed molecules after separation appear at points 3 and 4, respectively. On comparing the separated molecules with CV and TB, it was observed that points 1 and 3 have similar color and displacement, and the same situation also occurs for points 2 and 4; this indicates that the mixed molecules of TB and CV can be separated on GF membranes *via* paper separation. However, the separated molecules cannot be detected by the Raman microscopy system because of their low concentrations.

The Raman spectra obtained when the mixed solution of CV and TB is spotted on the MoS_2 substrate using a capillary tube are shown in Fig. 9b. Complex spectra appeared due to the presence of two molecules; therefore, the type of the molecule

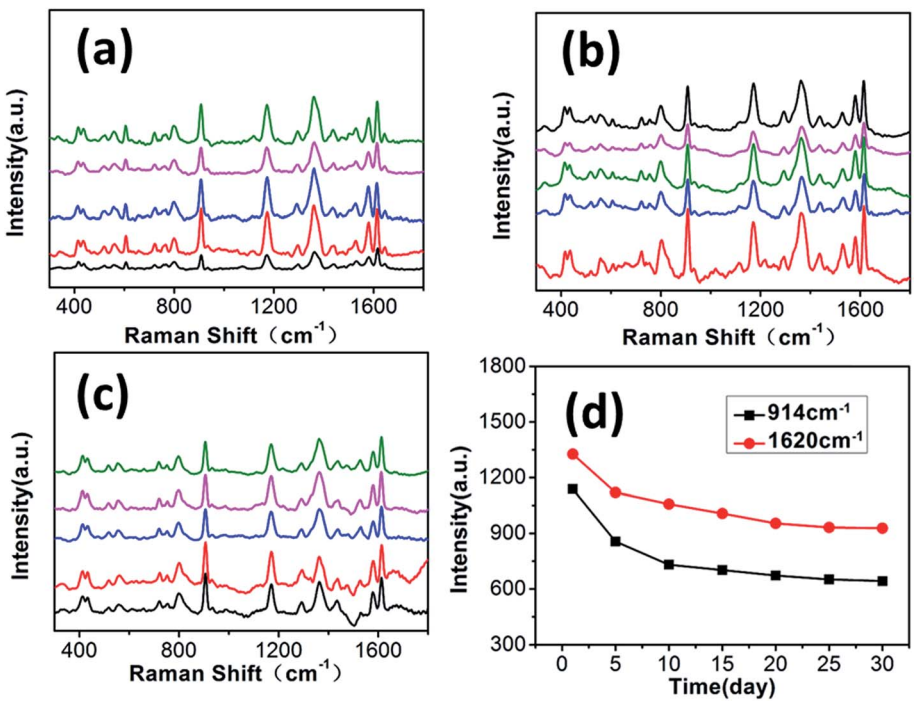

Fig. 8 (a)–(c) SERS spectra of CV (10^{-5} M) on the GF-MoS_2@AuNP-4 substrate recorded for five different spots on three different parts. (d) The Raman intensity changes of the peaks at 914 cm^{-1} and 1620 cm^{-1} with time.

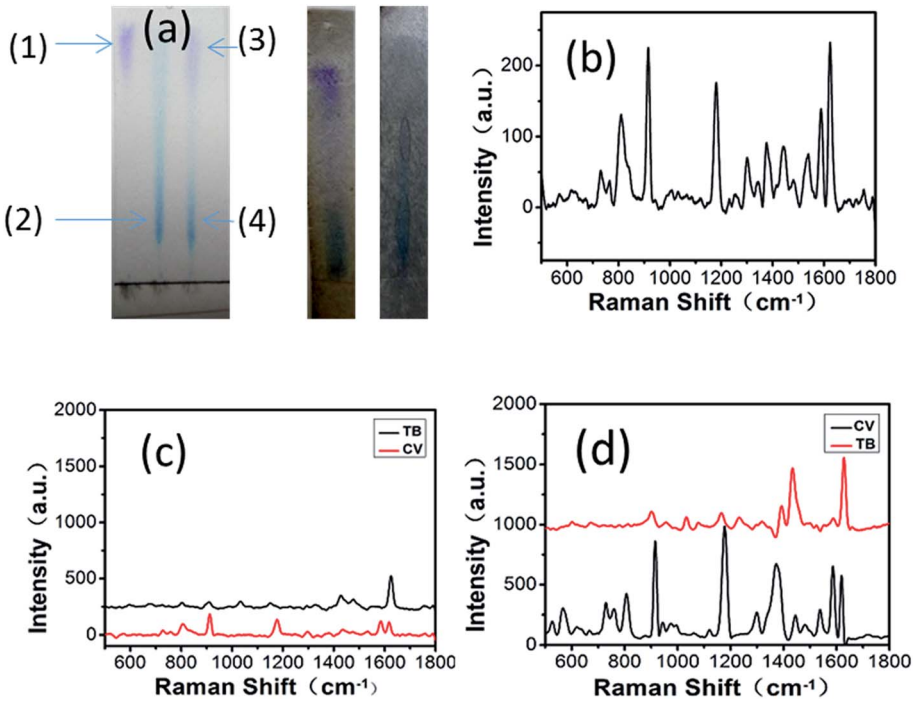

Fig. 9 (a) Colorimetric detection of dye molecules (CV, TB, and their mixed solution) after paper separation and images of the mixed solution after separation on the MoS_2 and GF-MoS_2@AuNP-4 substrates. The molecules of CV and TB are at the (1) and (2) positions. And the separated molecules of CV and TB from mixed solution are at the (3) and (4) positions. (b) Raman spectra of the mixed solution. (c) and (d) Raman spectra of the CV and TB molecules after paper separation on the MoS_2 and GF-MoS_2@AuNP-4 substrates.

cannot be determined. When mixed molecules are clearly distinguished after paper separation on the MoS_2 substrate, the two types of molecules can be determined separately and their Raman spectra can be obtained (Fig. 9c). According to the location of the characteristic peaks of CV and TB, it is clear that the two Raman spectra belong to CV and TB, respectively. The third image in Fig. 9a shows the images of the mixed solution after paper separation on the GF-MoS_2@AuNP-4 substrate. Compared with the second image, the distance between the two points after separation on the GF-MoS_2@AuNP-4 substrate is less. The reasons may be that separated molecules reside near the nanogap-rich AuNPs, which allow the plasmonic enhancement of the SERS signals. We can observe that Raman signals in Fig. 9d are much stronger than those in Fig. 9c because of the presence of AuNPs. Mixed small molecules can be successfully distinguished over both substrates and also detected by SERS measurement after paper separation. However, the GF-MoS_2@AuNP-4 substrate can achieve more sensitive detection of small molecules; thus, it can be used to separate and detect molecules with lower concentrations. When a lower concentration (10^{-8} M) of the mixed solution is separated on the substrate, although the color cannot be resolved, we can still detect their Raman spectra at their corresponding positions.

Conclusion

In conclusion, we obtained an efficient SERS-active substrate by synthesizing a GF-MoS_2@AuNP substrate with uniform and high density of AuNPs. Layered MoS_2 was applied to synthesize the AuNPs that enhanced the SERS signal *via* chemical adsorption. AuNPs are used to obtain the localized electric field enhancement. The GF membranes, which cannot be easily destroyed due to their thermal stability, are used to separate the mixed molecules. These GF-MoS_2@AuNP hybrid substrates show a huge potential for an excellent paper-based separation and are SERS-active substrates.

References

1 C. Yang, C. Zhang, Y. Huo, S. Jiang, H. Qiu, Y. Xu, X. Li and B. Man, *Carbon*, 2016, **98**, 526–533.
2 W. L. Barnes, A. Dereux and T. W. Ebbesen, *Nature*, 2003, **424**, 824–830.
3 K. Kneipp, H. Kneipp and J. Kneipp, *Acc. Chem. Res.*, 2006, **39**, 443–450.
4 M. M. Maye, J. Luo, L. Han and C.-J. Zhong, *Nano Lett.*, 2001, **1**, 575–579.
5 W. W. Yu and I. M. White, *Analyst*, 2013, **138**, 3679–3686.
6 C. Mueller, W. Weinmann, S. Dresen, A. Schreiber and M. Gergov, *Rapid Commun. Mass Spectrom.*, 2005, **19**, 1332–1338.
7 K. S. Minioti, C. F. Sakellariou and N. S. Thomaidis, *Anal. Chim. Acta*, 2007, **583**, 103–110.
8 N. Gogoi, M. Barooah, G. Majumdar and D. Chowdhury, *ACS Appl. Mater. Interfaces*, 2015, **7**, 3058–3067.
9 M. A. Farajzadeh and M. R. A. Mogaddam, *Anal. Chim. Acta*, 2012, **728**, 31–38.

10 B. Buszewski and S. Noga, *Anal. Bioanal. Chem.*, 2012, **402**, 231–247.
11 F. Karabiber, J. L. McGinnis, O. V. Favorov and K. M. Weeks, *RNA*, 2013, **19**, 63–73.
12 H. Wang, J. Liu, R. G. Cooks and Z. Ouyang, *Angew. Chem.*, 2010, **122**, 889–892.
13 H. Jung, M. Park, M. Kang and K.-H. Jeong, *Light: Sci. Appl.*, 2016, **5**, e16009.
14 S. Jiang, J. Guo, C. Zhang, C. Li, M. Wang, Z. Li, S. Gao, P. Chen, H. Si and S. Xu, *RSC Adv.*, 2017, **7**, 5764–5773.
15 H. Qiu, Z. Li, S. Gao, P. Chen, C. Zhang, S. Jiang, S. Xu, C. Yang and H. Li, *RSC Adv.*, 2015, **5**, 83899–83905.
16 J. Zhao, Z. Zhang, S. Yang, H. Zheng and Y. Li, *J. Alloys Compd.*, 2013, **559**, 87–91.
17 S. Su, C. Zhang, L. Yuwen, J. Chao, X. Zuo, X. Liu, C. Song, C. Fan and L. Wang, *ACS Appl. Mater. Interfaces*, 2014, **6**, 18735–18741.
18 E. Boisselier and D. Astruc, *Chem. Soc. Rev.*, 2009, **38**, 1759–1782.
19 S.-W. Joo, *Vib. Spectrosc.*, 2004, **34**, 269–272.
20 Y. W. Chen, T. Y. Liu, P. J. Chen, P. H. Chang and S. Y. Chen, *Small*, 2016, **12**, 1458–1468.
21 S. Najmaei, A. Mlayah, A. Arbouet, C. Girard, J. Léotin and J. Lou, *ACS Nano*, 2014, **8**, 12682.
22 A. M. Schwartzberg, C. D. Grant, A. Wolcott, C. E. Talley, T. R. Huser, R. Bogomolni and J. Z. Zhang, *J. Phys. Chem. B*, 2004, **108**, 19191–19197.
23 C. M. Cobley, J. Chen, E. C. Cho, L. V. Wang and Y. Xia, *Chem. Soc. Rev.*, 2011, **40**, 44–56.
24 C. Yang, Y. Xu, C. Zhang, Z. Sun, C. Chen, X. Li, S. Jiang and B. Man, *Nanoscale Res. Lett.*, 2014, **9**, 394.
25 X. Fang, S. Wei and J. Kong, *Lab Chip*, 2014, **14**, 911–915.
26 H. X. Gu, D. W. Li, L. Xue, Y. F. Zhang and Y. T. Long, *Analyst*, 2015, **140**, 7934.
27 K. Zhang, J. Zhao, H. Xu, Y. Li, J. Ji and B. Liu, *ACS Appl. Mater. Interfaces*, 2015, **7**, 16767.
28 T. Sreeprasad, P. Nguyen, N. Kim and V. Berry, *Nano Lett.*, 2013, **13**, 4434–4441.
29 S. Shao, Z. Chi, L. Yuwen, C. Jie, X. Zuo, X. Liu, C. Song, C. Fan and L. Wang, *ACS Appl. Mater. Interfaces*, 2014, **6**, 18735.
30 W. Kim, Y. H. Kim, H. Park and S. Choi, *ACS Appl. Mater. Interfaces*, 2015, **7**, 27910.